Volume 3
Number 4
21 February 2022
Pages 1837–2236

Materials Advances

rsc.li/materials-advances

ISSN 2633-5409

ROYAL SOCIETY OF CHEMISTRY

PAPER

Masataka Ohtani *et al.*
Impact of nanosizing a host matrix based on a metal–organic framework on solid-state fluorescence emission and energy transfer

Materials Advances

ROYAL SOCIETY OF CHEMISTRY

PAPER

View Article Online
View Journal | View Issue

Cite this: *Mater. Adv.*, 2022, 3, 2011

Impact of nanosizing a host matrix based on a metal–organic framework on solid-state fluorescence emission and energy transfer†

Hikaru Sakamoto, Akitaka Ito and Masataka Ohtani *

Received 11th November 2021,
Accepted 23rd December 2021

DOI: 10.1039/d1ma01056e

rsc.li/materials-advances

We demonstrate that the nanosize effect appears to affect the properties of dye molecules encapsulated in the pores of a metal–organic framework (dye@MOF). The emissive properties of the nano-sized dye@MOF are improved compared with those of sub-micron-sized dye@MOF. The fluorescence energy transfer between encapsulated dye molecules and adsorbed quencher molecules exhibits a higher efficiency with a smaller dye@MOF crystal compared with a larger dye@MOF crystal.

Introduction

Over the last few decades, several different strategies have been developed to improve the emissive properties of organic molecules in the solid state.[1–4] Among them, the encapsulation of emissive organic dye molecules in a porous host matrix is an attractive method. For example, nano- or mesoporous materials, such as zeolites, clay minerals, mesoporous silicas and dendrimers, are frequently used as a host matrix.[5–8] In the past, it has been reported that organic molecules adsorbed or encapsulated in a host matrix exhibit long-lived luminescence and higher emission quantum efficiency by suppressing the vibration or rotation of emitter molecules.[9–12] The relationship between fluorescence energy transfer efficiency of organic dyes adsorbed on the host surface and charge density has also been revealed.[13] In this context, host–guest interactions between the host matrix and guest emissive molecules are strongly affected by the host nanostructures, such as the crystal size, pore size/shape and framework components.

Calzaferri *et al.* conducted a numerical study in which several dyes were encapsulated in a zeolite as a host and reported that the emissive properties of each dye isolated in the pores of the zeolite were maintained to be the same as those in the solution state.[14] Tagaya *et al.* investigated the luminescence properties of organic dyes encapsulated in mesoporous silica with different pore sizes.[15] The aligned dyes in the pores showed higher emissive properties than the solid-state dyes owing to less influence from heating aggregation and concentration quenching. The synthesis and emissive properties of luminescent mesoporous organosilicas using chromophores as bridging organic groups have been reported.[15] Such fluorescent mesoporous materials exhibit efficient light absorption owing to the dense arrangement of chromophores in the framework. Because an organic chromophore can be introduced in the framework and/or mesopores of the materials, host–guest interactions between dyes in the framework and/or mesopores have been investigated.[16–19] Furthermore, the emissive dye-encapsulation strategy using mesoporous materials has also been applied to the hybridization of a photocatalytic system in mesoporous silica, which has resulted in the enhancement of photocatalytic performance and the durability.[20] Although there have been numerous reports using combinations of host porous materials and guest emissive and/or photoactive molecules, they are not sufficient to understand the relationship between the porous structure of the host matrix and the properties of the guests. It is necessary to construct the structure at the molecular level to reveal the interaction in detail.

Metal–organic frameworks (MOFs) are ideal host materials that can freely design a nanospace suitable for the incorporation of various dyes. The zeolitic imidazolate framework (ZIF) is one of the rapidly developing subclasses of MOFs.[21] The three-dimensional tetrahedral framework structure of ZIF consists of divalent metal cations and imidazolate anions. ZIF has various zeolite topologies such as SOD, LTA and FAU. It also has a huge specific surface area, comparable to zeolites, and high thermal and chemical stability.[22] Among them, ZIF-8, which consists of zinc(II) ions and 2-methylimidazole (2-HMIm), has been used as the host material in recent studies. For example, Glembockyte *et al.* found that single molecules encapsulated in a rigid ZIF-8 nanospace exhibited emissive properties similar to those of solution-state dyes, even though they were in the solid state.[23,24] However, the influence of the nanostructure on the host–guest

School of Environmental Science and Engineering, Kochi University of Technology, 185 Miyanokuchi, Tosayamada, Kami, Kochi 782-8502, Japan.
E-mail: ohtani.masataka@kochi-tech.ac.jp

† Electronic supplementary information (ESI) available. See DOI: 10.1039/d1ma01056e

interaction through a MOF nanospace has yet to be clarified. In this study, we focus on the nanometre-scale size effect of a MOF crystal on the emissive properties of encapsulated dye molecules.

Results and discussion

Nanosizing of a metal–organic framework

First, we attempt to control the crystal size of ZIF-8 by focusing on the synthetic conditions. Although several factors affect the size, shape and crystallinity of ZIF-8, we consider four critical factors. The first is the solvent used for the reaction. The formation process of ZIF-8 is strongly influenced by the polarity of the solvent because it is an equilibrium reaction between metal ions and organic ligands. Second, the reaction temperature is an important factor in the nucleation and crystal growth processes. Usually, crystals obtained at high temperatures tend to be large and highly crystalline. Third is the competing ligand. It is known that a modulator, such as sodium formate and 1-methylimidazole (1-MIm), competes with the bridging ligands for the metal ions and influences the reaction rate between metal ions and the bridging ligand in the process of nucleation and crystal growth.[21] The last is ligand activation. In particular, deprotonation of the imidazole ligand influences the equilibrium reaction that is not controlled by the solvent or reaction temperature.

We first investigated the effect of the solvent on the crystal size control of ZIF-8. We used protic solvents such as methanol (MeOH), ethanol and ethylene glycol (EG), and aprotic solvents such as acetonitrile (MeCN), *N*,*N*-dimethylformamide (DMF) and their mixtures. Zinc(II) nitrate and 2-methylimidazole (2-HMIm) were dissolved in the solvent at the molar ratio (metal ion : ligand) of 1 : 4 and mixed at room temperature and atmospheric pressure. The powdery products were collected by centrifugation, washed and dried *in vacuo*. The crystal phase and crystallinity of the products were confirmed by powder X-ray diffraction (PXRD). As shown in Fig. S1 (ESI†), the PXRD patterns of all products matched with the simulated diffraction pattern of a ZIF-8 single crystal (CCDC: 864309). To confirm the size and shape of these ZIF-8 crystals, we performed an analysis by using scanning electron microscopy (SEM). SEM images revealed that only methanol and ethylene glycol gave crystals with uniform rhombohedral dodecahedra (Fig. 1a and e), with respective crystal sizes (d) of d_{MeOH} = 470 nm and d_{EG} = 590 nm. When other alcoholic solvents instead of methanol were used, aggregated bulk crystals were obtained (Fig. 1b and Fig. S2, ESI†). However, when aprotic nitrile solvents were used, nanocrystals with diameters in the range of 20 nm to 60 nm were obtained (Fig. 1c and d). In the case of benzonitrile, spherically aggregated secondary particles were formed (Fig. S3, ESI†). In addition, although DMF is a highly polar aprotic solvent, the reaction using DMF at room temperature did not yield any product. Furthermore, similar reactions were also conducted using mixed solvents with the combination of protic/protic solvent (EG and MeOH) and aprotic/protic solvent (MeCN and MeOH). According to the series of SEM images, the crystal size of the obtained ZIF-8 decreased in the case of a higher mixing ratio of EG in MeOH (Fig. S4, ESI†). This trend was also observed in the case of a MeCN–MeOH mixed solvent (Fig. S2b, ESI†). These results suggest that the choice of solvent affects the size, shape and aggregation of ZIF-8. In particular, MeOH and MeCN are suitable for the preparation of uniform and crystalline ZIF-8 in the size range of micrometres to nanometres.

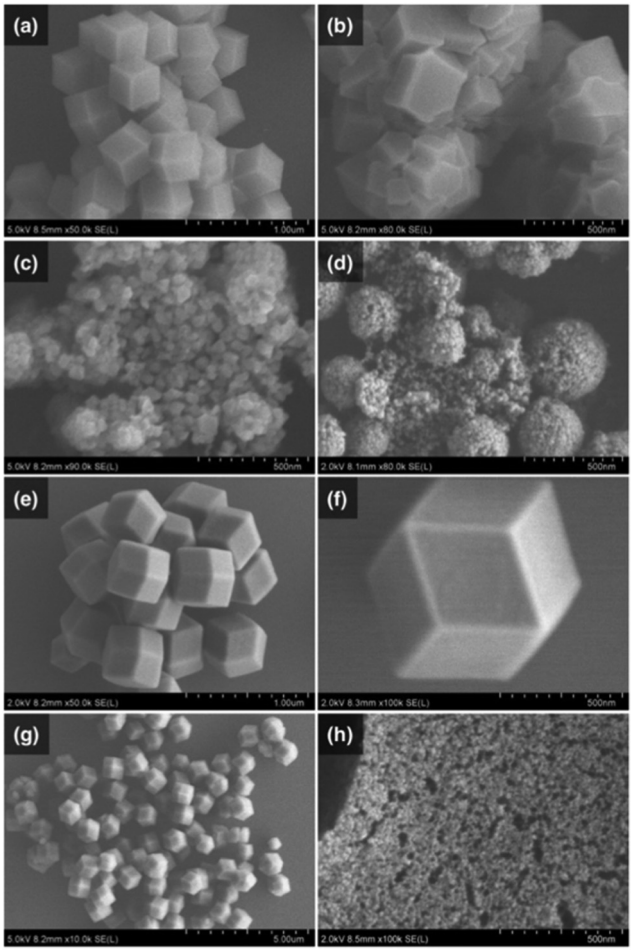

Fig. 1 SEM images of ZIF-8 synthesized under different conditions: (a) methanol; (b) ethanol; (c) acetonitrile; (d) benzonitrile; (e) ethylene glycol; (f) methanol (4 °C); (g) methanol (the precursor zinc solution without 1-MIm) and (h) methanol with addition of triethylamine (1-eq. amount based on 2-HMIm).

Because the size of ZIF-8 obtained by using MeOH was submicrometre, we also confirmed the temperature effect on the crystal growth progress of ZIF-8 to obtain ZIF-8 crystals larger than micrometre size. Generally, the reaction at high temperature tends to provide larger sized and highly crystalline products. Therefore, similar experiments were conducted by using precursor solutions heated *via* a hot plate. In contrast to our expectations, 250 nm scale crystals were obtained (Fig. S5a, ESI†). In the case of using a precursor cooled by ice water, 1 μm or larger crystals were obtained (Fig. 1f and Fig. S5b, ESI†). The effect of the reaction temperature was also investigated

using other alcoholic and nitrile solvents. Regardless of the solvent type, the crystal size tended to be larger when the reaction temperature was lower than room temperature and yielded smaller crystals at higher temperature (Fig. S2 and S3, ESI†). According to XRD results, the products obtained at different reaction temperatures showed similar crystallinity to ZIF-8 obtained at room temperature conditions. As there was no difference in the product yield of ZIF-8 in each condition, it was considered that the reaction temperature accelerated the nucleation rate at the initial stage of reaction. The size of the ZIF-8 crystal could be controlled in the range of 20 nm to 1 μm by changing the solvents and reaction temperature.

In addition to the particle size, a uniform size and shape of ZIF-8 crystals is a very important structural factor in the use of ZIF-8 as a host material. We investigated whether the presence of the competing ligand in the precursor solution was the key to controlling the crystal shape in terms of equilibrium reactions between metal ions and ligands. 1-MIm was used as a competing ligand in the reaction system. According to the reported method (Method 1),[21] ZIF-8 was synthesized by adding a precursor of dissolved 1-MIm and 2-HMIm to a zinc solution. The product was observed to have a rhombic dodecahedron shape from the SEM images, but the crystal size varied (d = 960 ± 200 nm, Fig. 1g). For comparison with Method 1, the precursor of dissolved 2-HMIm was added to the solution of dissolved 1-MIm and zinc(II) ions (Method 2). SEM images showed that the product obtained by Method 2 was a nanocrystal with uniform size and shape (d = 470 ± 25 nm, Fig. 1a and Fig. S6a, ESI†). As a result, the standard deviation of ZIF-8 in Method 2 was smaller than that in Method 1. This was attributed to the fact that the 1-MIm coordinated to the zinc ion behaves as a protecting group. As a method to obtain crystals with a small standard deviation, the use of competing ligands that affect the reaction between metal ions and bridging ligands was found to be effective.

We hypothesized that a smaller size of the host material will result in a stronger host–guest interaction. To obtain a crystal size below 20 nm, which had not been achieved by changing the reaction temperature and solvent, we investigated the effect of triethylamine (TEA) as a base on the crystallinity and crystal size of ZIF-8. TEA (1-equivalent mole to that of zinc ions) was added to the precursor solution containing the 2-HMIm ligand. In the case of using TEA, the reaction solution immediately became cloudy after mixing. As a result, substantially smaller ZIF-8 nanocrystals (d_{TEA} = 9 nm) were observed from the SEM image (Fig. 1h). The product yield was also five times greater than that without TEA. The crystal size of ZIF-8 could be finely controlled in the range from 9 nm to 30 nm with different additive amounts of TEA (Fig. S7a–c, ESI†). The PXRD results showed that TEA used as a deprotonating agent for 2-HMIm did not affect the crystallinity of ZIF-8 (Fig. S7d, ESI†). Nitrogen adsorption isotherm measurements were performed to investigate the surface area and porosity of ZIF-8 samples with different crystal sizes obtained by various synthesis methods. As shown in Fig. S8 and Table S2 (ESI†), there was no significant difference in their specific surface area and pore volume, indicating that the nanosized ZIF-8 maintained their crystallinity and porosity without increasing the crystal defect and amorphized part.

Encapsulation of a fluorescent dye in the nano-sized MOF crystal

Focusing the synthetic parameter in the above-mentioned study, a method for controlling the crystal size of ZIF-8 in the range from 9 nm to 1 μm while maintaining the high crystallinity has been developed (Table S1, ESI†). As described in the Introduction, size-controlled ZIF-8 is an attractive host material. There are two approaches to introducing organic dyes into the pores of ZIF-8. The first is to disperse ZIF-8 and organic dyes together in a solution. In this method, the dye molecules must be smaller than the opening diameter of the ZIF-8 pores. We also need to be careful that the dyes do not leak out. The second method is to introduce the organic dye into the pores during the formation of the ZIF-8 framework. It is possible to introduce dye molecules with a size equivalent to the pore inner diameter. We adopted the method of pre-dissolving organic dyes in the precursor solution because it has less chance of dye leakage from the pores. Here, 8-(phenylamino)-1-naphthalenesulfonic acid (ANS) was selected as a guest molecule, because the encapsulated ANS in the cavities of ZIF-8 would not escape from the pores because of its larger size than the opening diameter of the ZIF-8 pore. In addition, because ANS exhibits different emissive properties in the solid state and solution state (Fig. 2a and e), we assumed that a clear difference of the dye state could be observed after encapsulation in the pores of the ZIF-8 host from its emissive properties.

The synthetic methodology consisted of the same procedure except that ANS was added to the precursor solution containing zinc and 1-MIm. The dark green coloured precursor solution

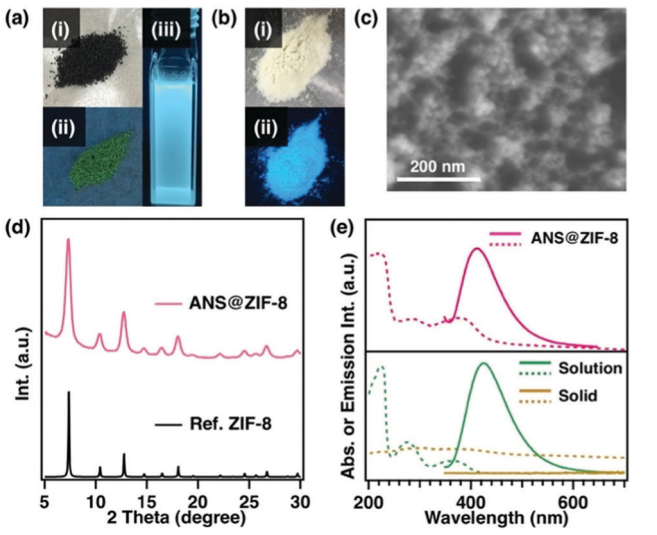

Fig. 2 Photographs of solid-state ANS under visible light (a-i), under UV light (a-ii), ANS solution in MeCN under UV light (a-iii), ANS@ZIF-8 under visible light (b-i) and under UV light (b-ii). (c) SEM image of ANS@ZIF-8. (d) XRD pattern of ANS@ZIF-8 (pink) and a simulated ZIF-8 reference (black). (e) UV-vis absorption (dot line) and fluorescence (solid line) spectra of ANS@ZIF-8 in the solid state (pink), ANS in the MeCN solution state (green) and ANS in the solid state (yellow).

was added to the solution containing 2-HMIm and TEA. The product was washed several times with various solvents to separate the unreacted dye. Even after exhaustively washing the greenish powdery product with several kinds of solvents, the greenish colour of the powder did not change, which indicated that ANS was encapsulated deep within the ZIF-8 crystals (Fig. 2b). To confirm the encapsulation of ANS inside the ZIF-8 pores, ANS@ZIF-8 was analysed by several methods. Comparison with the results of PXRD revealed that encapsulation of ANS within ZIF-8 did not affect the crystal structure (Fig. 2d). From an SEM image, the crystal size of the product was 13 nm (Fig. 2c). The solid-state ANS@ZIF-8 emitted blue light under UV light irradiation, the same emission colour as the ANS solution (Fig. 2a-iii and b-ii). Therefore, the ANS@ZIF-8 crystal exhibited blue fluorescence that originated from ANS under UV light irradiation.

To investigate the emission properties of ANS@ZIF-8 in more detail, absorption/emission spectroscopy was performed. ANS@ZIF-8 showed a similar adsorption spectrum to that of the dye in solution, with three peaks at 220, 280 and 360 nm. The emission spectrum of ANS@ZIF-8 was also similar to that of the dye in solution. The amount of dye encapsulated in ZIF-8 was determined by scanning transmission electron microscopy-energy dispersive X-ray spectroscopy (STEM-EDX). According to the STEM-EDX analysis, the content of sulphur arising from ANS was detected at 1 atomic% (at%) relative to the Zn-ion in ZIF-8 (Fig. 3), denoted as ANS(1%)@ZIF-8.

To study the emissive behaviour of ANS encapsulated in ZIF-8, we prepared nanosized ZIF-8 including 1 at% to 3 at% of sulphur at different mole ratios of ANS (0.05 mmol to 0.25 mmol) in the precursor solution (Fig. 3a). XRD showed that the ZIF-8 structure was unaffected by the amount of ANS incorporated (Fig. S9, ESI†). From the UV-vis absorption and emission spectra, the wavelengths of maximum absorption/emission of ANS (2 at% or 3 at%) @ ZIF-8 were also very similar to those of the ANS solution. As the amount of ANS encapsulated in the nanosized ZIF-8 increased, the emission intensity and efficiency decreased (Fig. 3b). This phenomenon was concentration quenching, which generally occurs in solution. Moreover, in terms of the relationship between the pore size of ZIF-8 and the size of organic molecules, the dyes as a single molecule are assumed to be encapsulated in the channels of ZIF-8. From N_2 adsorption measurements in Fig. S10 and Table S3 (ESI†), there was no significant difference in their surface area and pore volume. Thus, the organic dyes are not introduced at a high enough concentration to fill the total pores of ZIF-8. In addition, the N_2 adsorption behaviour of ANS@ZIF-8 with different crystal sizes (*ca.* 14 nm and 100 nm) was consistent with that of ZIF-8, indicating that the pore regularity of ZIF-8 with controlled sizes and dye encapsulation were not different. These results suggest that the organic dyes are sufficiently isolated from each other and distributed in the pore as a single molecule at a low concentration.

Effect of nanosizing on fluorescence efficiency of the dye@MOF

Furthermore, to examine the effect of the crystal size of ZIF-8 on the emissive properties of ANS encapsulated in the pores, we aimed to synthesize ZIF-8 with different crystal sizes while maintaining the inclusion amount of ANS. To obtain larger ZIF-8 crystals that encapsulated 1% of ANS, the sample was prepared by exploiting the effects of solvent and temperature. The product was light green in colour after several washes. PXRD revealed that the diffraction pattern of the product was consistent with the crystal structure, the same as that of nanosized ZIF-8 crystal encapsulated dyes. The TEM image showed that the crystal size of ANS@ZIF-8 was 130 nm. In addition, STEM-EDX was performed to clarify the inclusion of ANS molecules and their distribution in the ZIF-8 crystal. As a result, it was confirmed that 1% of S was distributed over the whole region of the crystal. The 130 nm-sized ANS(1%)@ZIF-8 emitted cyan colour under UV light irradiation, which was different from the 13 nm-sized ANS (1%)@ZIF-8 and ANS solution (Fig. 4a, 2a and b). From the absorption spectrum measurements, the absorption spectrum of ANS@ZIF-8 was observed to be similar to that of the dye in solution, with three peaks at 220, 280 and 360 nm. The 130 nm-sized ANS(1%)@ZIF-8 exhibited a substantially lower emission intensity compared with that of the 13 nm-sized ANS@ZIF-8. In addition, the broad peak of the 130 nm-sized ANS@ZIF-8 was slightly shifted to the longer wavelength side. This was consistent with the fact that the sample emitted cyan colour under UV light. Furthermore, as compared with the fluorescence quantum efficiency (QY, φ_{FL}) determined *via* an absolute method using an integrating sphere, the quantum yield of 13 nm-sized ANS@ZIF-8 (QY = 18%) was 9 times higher than that of 130 nm-sized ANS@ZIF-8 (QY = 2%).

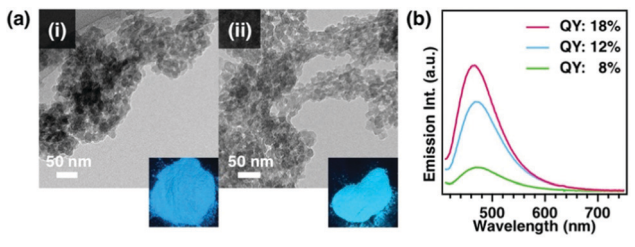

Fig. 3 (a) TEM images (insets show photographs under UV irradiation) and (b) solid-state fluorescence emission spectra of 13 nm-sized ANS@ZIF-8 with different contents of ANS: (i, pink) 1 at%; (ii, blue) 2 at%; (iii, green) 3 at% based on the Zn-ion content in ZIF-8.

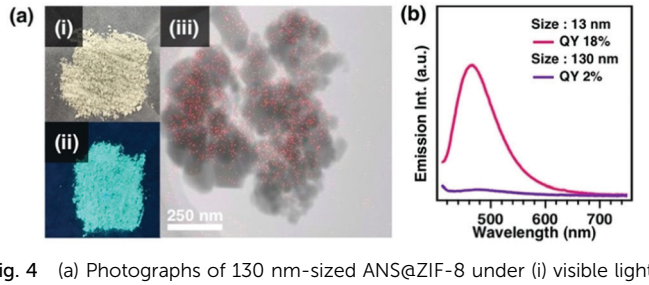

Fig. 4 (a) Photographs of 130 nm-sized ANS@ZIF-8 under (i) visible light and (ii) UV light (λ = 350 nm), and (iii) STEM image (grayscale) overlaid with sulphur element mapping by EDX (red). (b) Solid-state fluorescence spectra for ANS@ZIF-8 samples upon excitation at 375 nm: crystal sizes are 13 nm (pink) and 130 nm (violet).

The enhancement of the luminescence properties observed for ANS encapsulated in nanosized ZIF-8 is not unique to the combination of ANS and ZIF-8. To confirm the phenomenon, a similar experiment was performed with different types of organic dyes. Rhodamine B (RhB) was chosen because the size of the RhB molecule is larger than the opening diameter of the ZIF-8 pore and it exhibits different emissive properties in the solid state and solution (Fig. S11, ESI†). The initial concentration of RhB in the precursor solution was assumed to be the amount of RhB loaded in RhB@ZIF-8 (Fig. S12–S14, ESI†). The emissive properties of RhB encapsulated in nanosized ZIF-8 were superior to those of sub-nanosized RhB@ZIF-8 (Fig. S15 and S16, ESI†). This was very similar to the emissive behaviour of ANS@ZIF-8. In particular, the comparison of the quantum yields of RhB@ZIF-8 having various crystal sizes revealed that the quantum yield of RhB encapsulated in the smallest ZIF-8 was the highest (Fig. S16, ESI†). Therefore, the nanometre-scale size effect is a universal phenomenon that affects the luminescence properties of any molecule encapsulated in a pore.

We consider the following reasons why the nanosized host improves the solid-state emissive properties of the encapsulated organic dye. Generally, the emission intensity and efficiency of dyes in the solid state tend to decrease owing to interactions with themselves or external factors. Light absorption of organic dyes encapsulated in porous materials is also greatly hindered by light scattering effects owing to the side wall and surface structure of the host materials. Accordingly, in the case of a larger dye-encapsulated ZIF-8 crystal, it is assumed that the thick crystal and rough surface cause scattering of excitation light. In addition, the roughness in the gap of the aggregation made from a large number of ZIF-8 crystals with different crystal sizes affects the light scattering. In contrast to this, organic dyes encapsulated in smaller nanocrystals showed higher luminescence properties, as shown in Fig. 3b. This suggests that there is no significant light scattering owing to the thin wall and nanosized roughness of the host ZIF-8 nanocrystal, resulting in the enhancement of light outcoupling efficiency in the fluorescence process. Additionally, the absolute number of dye molecules present in one nanosized crystal is very small, which probably reduces the effect of the thermal nonradiative deactivation process and concentration quenching caused among dyes and/or between a dye and a host crystal lattice. These effects were mitigated by the nanosizing of the MOF crystals, affecting the fraction of the rate constants of fluorescence transition, nonradiative deactivation (QY: $\varphi_{FL} = k_{FL}/(k_{FL} + \Sigma k_{nr})$).[9,14,19,25,26] Although it is difficult to prove the mechanism without directly observing the luminescence phenomenon from *ca.* 10 nm-sized crystals and their dynamics, it is believed that a combination of several factors caused the strong luminescence enhancement from nanosized host crystals.

Fluorescence resonance energy transfer through the nanospace of the dye@MOF nanocrystal

We observed that the crystal size of the host, ZIF-8, affects other properties in addition to the emission intensity and efficiency of the encapsulated dye molecules. The efficiency of fluorescence resonance energy transfer (FRET) strongly depends on the distance between donor and acceptor (r), especially in the range of 3 nm to 10 nm. It has been reported that FRET occurs with high efficiency when acceptor molecules are regularly arranged on mesoporous organosilicas as a host.[15] The effect of crystal size was investigated by observing the FRET between donor and acceptor molecules through the ZIF-8 nanospace ($r = d/2$). We used the quenching phenomenon between two molecules, RhB encapsulated in the pores as a donor molecule and malachite green (MG) adsorbed on the crystal surface as an acceptor molecule (Fig. S17–S20, ESI†). Compared with the emission behaviour of MG-RhB@ZIF-8 crystals with different crystal sizes, the quenching efficiency of the 16 nm-sized MG-RhB@ZIF-8 crystal increased with an increasing amount of MG (Fig. 5i, ii and Table S4, ESI†). Furthermore, the Stern–Volmer plot of the quenching efficiency *versus* quencher concentration[27] shows that the quenching efficiency of 16 nm-sized RhB@ZIF-8 was approximately two times higher than that of 75 nm-sized RhB@ZIF-8 (Fig. 5b). This result indicates that the smaller crystals closer to the crystal interface exhibit a higher FRET efficiency. The ''nanometre-scale size effect'' of ZIF-8 was also shown to affect other properties of the guest molecules encapsulated in the pores. To examine the mechanism in detail, it is necessary to analyse the emissive properties for one isolated ZIF-8 nanocrystal with 10 nm size to verify the mechanism of the phenomenon.

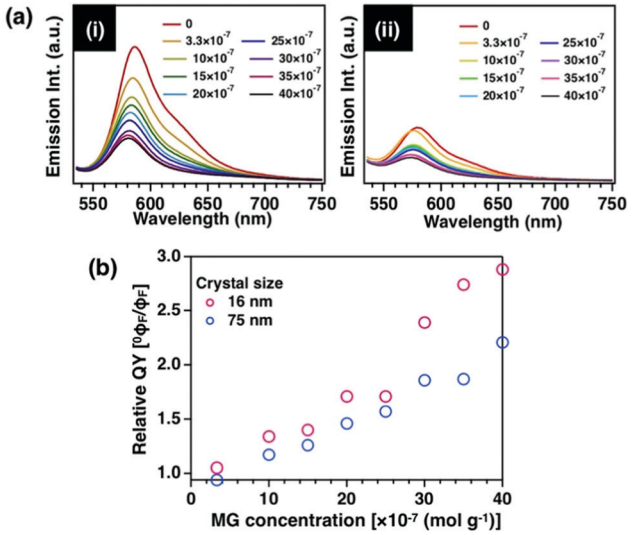

Fig. 5 (a) Fluorescence quenching in the solid-state fluorescence emission spectra of RhB@ZIF-8 with different crystal sizes (i: 16 nm, ii: 75 nm) by adding MG as a quenching agent and (b) Stern–Volmer plot for fluorescence quenching of RhB@ZIF-8 related to MG content.

Conclusions

In conclusion, nanosized ZIF-8 crystals are shown to be attractive host materials for the encapsulation of dye molecules. By focusing on nucleation and crystal growth rate, we succeed

in controlling the crystal size of ZIF-8 in a range from nanometre-scale to micrometre-scale while maintaining its crystallinity. The crystal size of the ZIF-8 affects not only the emissive properties of the encapsulated guest molecules in pores but also the efficiency of energy transfer. It is expected that the nanometre-scale size effect also affects other properties such as catalytic performance, adsorption, and conductivity, for example. Furthermore, it has been reported that ZIF-8 can self-assemble into superstructures, such as photonic crystals, by precisely controlling its shape and crystal size.[2] We expect to develop photo energy-transfer systems that exhibit efficient FRET by arranging and self-assembling superstructures using nanosized ZIF-8.

Experimental

Materials

All the reagents and chemicals used were obtained from commercial sources and used as received, unless otherwise noted. Methanol (MeOH), ethanol (EtOH), 1-propanol (1-PrOH), 2-propanol (2-PrOH), *n*-butanol (*n*-BuOH), acetonitrile (MeCN), propionitrile, benzonitrile, zinc(II) nitrate hexahydrate ($Zn(NO_3)_2{\cdot}6H_2O$), 1-methylimidazole (1-MIm), 2-methylimidazole (2-HMIm), triethylamine (TEA), *N*,*N*-diisopropylethylamine, 1,8-diazabicyclo-[5,4,0]undec-7-ene, rhodamine B (Rh B), malachite green, oxalate (MG), and 8-(phenylamino)-1-naphthalenesulfonic acid (ANS) were purchased from Wako Pure Chemical Industries Co. Ltd.

Synthetic procedure of ZIF-8 with different crystal sizes

Effect of reaction solvent. 734.4 mg (2.47 mmol) of $Zn(NO_3)_2{\cdot}6H_2O$ and 810.6 mg (9.87 mmol) of 1-MIm were dissolved in solvent (50 mL). MeOH, EtOH, 1-PrOH, 2-PrOH, *n*-BuOH, MeCN, propionitrile, and benzonitrile are used as a reaction solvent. A second solution is prepared by dissolving 810.6 mg (9.87 mmol) of 2-HMIm in solvent (50 mL). The latter clear solution is poured into the former clear solution under stirring with a magnetic stirrer (25 °C, 5 min). After 24 h, the product is centrifuged (9000 rpm, 15 min), washed several times with MeOH or MeCN, and dried under vacuum (30 °C, 24 hours) to give a powdery product (white powder).

Effect of reaction temperature. 734.4 mg (2.47 mmol) of $Zn(NO_3)_2{\cdot}6H_2O$ and 810.6 mg (9.87 mmol) of 1-MIm were dissolved in solvent (50 mL: MeOH, EtOH, 1-PrOH, 2-PrOH, *n*-BuOH, MeCN, propionitrile, benzonitrile). A second solution is prepared by dissolving 810.6 mg (9.87 mmol) of 2-HMIm in solvent (50 mL). These solutions are pre-warmed on an electric hot plate or ice-water bath until they reach the reaction temperature. After that, the latter clear solution is poured into the former clear solution at 4 °C per room temperature/temperature below the boiling point of each solvent under stirring. After 1 hour, stirring is stopped and the solution is left to stand at room temperature overnight. The product is centrifuged (9000 rpm, 15 min), washed several times with MeOH or MeCN, and dried under vacuum (30 °C, 24 hours) to give a powdery product (white powder).

Effect of base addition. 734.4 mg (2.47 mmol) of $Zn(NO_3)_2{\cdot}6H_2O$ and 810.6 mg (9.87 mmol) of 1-MIm were dissolved in MeOH (50 mL). A second solution was prepared by dissolving 810.6 mg (9.87 mmol) of 2-HMIm and 249 mg (2.47 mmol) of TEA in MeOH (50 mL). The latter clear solution was poured into the former clear solution under stirring with a magnetic stirrer (25 °C, 5 min). After 24 h, the obtained mixture was centrifuged (9000 rpm, 15 min), washed several times with MeOH and MeCN, and dried under vacuum (30 °C, 24 hour) to give a powdery product (white powder).

Synthesis of size-controlled organic dye@ZIF-8. 734.4 mg (2.47 mmol) of $Zn(NO_3)_2{\cdot}6H_2O$ and 810.6 mg (9.87 mmol) of 1-MIm, organic dye (0.25 mmol, RhB or ANS) were dissolved in MeCN (50 mL). A second solution was prepared by dissolving 810.6 mg (9.87 mmol) of 2-HMIm and 249 mg (2.47 mmol) of TEA in MeCN (50 mL). The latter clear solution is poured into the former clear solution under stirring with a magnetic stirrer. After 24 h, the obtained mixture was centrifuged (9000 rpm, 15 min), washed 7 times with MeCN, and dried under vacuum (30 °C, 24 hour) to give a powdery product. Regardless of the type of organic dye, submicron-sized organic dye@ZIF-8 samples are obtained by cooling the reaction solvent at 4 °C.

Analytical methods

Scanning electron microscopy. Scanning electron microscopy (SEM) images were measured on a Hitachi FE-SEM SU-8020 microscope. A specimen was prepared by drop-casting of the dispersion of the crystal on a silicon wafer.

Transmission electron microscopy. Transmission electron microscopy (TEM) images were measured on a JEOL JEM-2100F microscope. For the preparation of the specimen, first, the powdery sample was dispersed in MeOH with sonication (30 min). Then, 5 μL of resultant dispersion was drop-casted on a carbon-coated copper micro grid and the solvent was vaporized under atmospheric conditions.

Powder X-ray diffraction (XRD) measurements. Powder X-ray diffraction (XRD) measurements were performed using a Rigaku SmartLab diffractometer with graphite-monochromatized Cu-K_α radiation (X-ray wavelength: 1.5418 Å) in steps of 0.02° over the 2θ range of 5–90°. A sample was set in a non-refractive silicon holder (Overseas X-Ray Service, Saitama, Japan).

Photophysical measurements. The UV-Vis absorption spectra of size-controlled organic dye@ZIF-8 samples were collected on a JASCO V-650 UV-Vis spectrophotometer and recorded from 250 nm to 700 nm. The measurements for the solution samples were performed using a 10 mm path length quartz cuvette. The solid-state measurements were conducted using an integrated sphere.

Steady-state emission spectra were recorded using a JASCO FP-8300 spectrophotometer with a Xe flash lamp. The fluorescence experiments were performed at room temperature, a scan speed of medium, an excitation slit width of 5 nm, and an emission slit width of 5 nm. The fluorescence emission spectra were recorded in the wavelength range of 540–800 nm upon excitation at 550 nm.

Fluorescence quantum yield measurements were conducted using a photoluminescence quantum efficiency measurement system (Hamamatsu C13534-01) equipped with an integrating sphere. The powdery samples of the dye@ZIF-8 were placed on quartz glass cups and covered with a quartz lid. In the case of RhB@ZIF-8 solids, excitation was performed at 550 nm and emission integration was performed in the range of 530 nm to 800 nm. In the case of ANS@ZIF-8 solids, excitation was performed at 375 nm and emission integration was performed in the range of 380 nm to 750 nm. Data were analysed using dedicated software (Hamamatsu U6039-05).

Fluorescence quenching experiment. 30 mg of 16 nm- or 75 nm-sized RhB@ZIF-8 were placed in a mortar and ground by hand. Then, MG solutions prepared to each concentration (3–40 mol g^{-1}, in MeCN) were dropped onto the samples and stirred until the MeCN evaporated. RhB@ZIF-8 samples with different amounts of MG adsorbed were dried under vacuum (30 °C, 24 hours).

Nitrogen adsorption isotherms. Nitrogen sorption isotherms were obtained at liquid nitrogen 77 K using BELSORP-mini II instrument (MicrotracBEL Corp.). Before the measurements, the samples were degassed under reduced pressure (<10 Pa) at 200 °C for 18 h.

Author contributions

Hikaru Sakamoto: data curation, formal analysis, investigation, methodology, visualization, writing – original draft, writing – review & editing; Akitaka Ito: data curation, formal analysis, investigation, and methodology; Masataka Ohtani: conceptualization, funding acquisition, formal analysis, investigation, methodology, project administration, resources, supervision, writing – original draft, writing – review & editing.

Conflicts of interest

There are no conflicts to declare.

Acknowledgements

We acknowledge the financial support from JSPS KAKENHI Grant number 19K05186. We thank Edanz (https://jp.edanz.com/ac) for editing a draft of this manuscript.

Notes and references

1 S. Nakajima, K. Albrecht, S. Kushida, E. Nishibori, T. Kitano, T. Uemura, K. Yamamoto, U. H. F. Bunz and Y. Yamamoto, *Chem. Commun.*, 2018, **54**, 2534–2537.
2 C. Avci, I. Imaz, A. C-Sanchez, J. A. Pariente, N. Tasios, J. P-Carvajal, M. I. Alonso, A. Blanco, M. Dijkstra, C. Lopez and D. Maspoc, *Nat. Chem.*, 2018, **10**, 78–84.
3 P. Miluski, M. Kochanowicz and J. Zmojda, *J. Optoelectron. Mater.*, 2017, **19**, 379–383.
4 C. Li, J. Cho, K. Yamada, D. Hashizume, F. Araoka, H. Takezoe, T. Aida and Y. Ishida, *Nat. Commun.*, 2015, **6**, 8418.
5 M. Sohmiya, K. Saito and M. Ogawa, *Sci. Technol. Adv. Mater.*, 2015, **16**, 54201–54218.
6 J. V. Morabito, L. Y. Chou, Z. Li, C. M. Manna, C. A. Petroff, R. J. Kyada, J. M. Palomba, J. A. Byers and C. K. Tsung, ***J.** Am. Chem. Soc.*, 2014, **136**, 12540–12543.
7 D. R. Godhani, H. D. Nakum, D. K. Parmar, J. P. Mehta and N. C. Desai, *J. Mol. Catal. A: Chem.*, 2017, **426**, 223–237.
8 K. Sakamoto, Y. Takashima, N. Hamada, H. Ichida, H. Yamagichi, H. Yamamoto and A. Harada, *Org. Lett.*, 2011, **13**, 672–675.
9 H. Mieno, R. Kabe, N. Notsuka, M. D. Allendorf and C. Adachi, *Adv. Opt. Mater.*, 2016, **4**, 1015–1021.
10 H. N. Abdelhamid, Z. Huang, A. M. E. Zohry, H. Zheng and X. Zou, *Inorg. Chem.*, 2017, **56**, 9139–9146.
11 H. Mieno, R. Kabe, M. D. Allendorf and C. Adachi, *Chem. Commun.*, 2018, **54**, 631–634.
12 H. Mieno, R. Kabe and C. Adachi, *Commun. Chem.*, 2018, **1**, 27.
13 M. Tominaga, Y. Oniki, S. Mochida, S. Tani, Y. Suzuki and J. Kawamata, *J. Phys. Chem. C*, 2016, **120**, 23813–23822.
14 G. Calzaferri, S. Huber, H. Maas and C. Minkowski, *Angew. Chem., Int. Ed.*, 2003, **42**, 3732–3758.
15 S. Inagaki, O. Ohtani, Y. Goto, K. Okamoto, M. Ikai, K. Yamanaka, T. Tani and T. Okada, *Angew. Chem., Int. Ed.*, 2009, **48**, 4042–4046.
16 D. Chadra, T. Yokoi, T. Tatsumi and A. Bhaumik, *Chem. Mater.*, 2007, **19**, 5347–5354.
17 Y. Goto, N. Mizoshita, O. Ohtani, T. Okada, T. Shimada, T. Tani and S. Inagaki, *Chem. Mater.*, 2008, **20**, 4495–4498.
18 J. Jia, L. Gutiérrez-Arzaluz, O. Shekhah, N. Alsadun, J. Czaban-Jóźwiak, S. Zhou, O. M. Bakr, O. F. Mohammed and M. Eddaoudi, *J. Am. Chem. Soc.*, 2020, **142**, 8580–8584.
19 L. Gutiérrez-Arzaluz, J. Jia, C. Gu, J. Czaban-Jóźwiak, J. Yin, O. Shekhah, O. M. Bakr, M. Eddaoudi and O. F. Mohammed, *J. Phys. Chem. Lett.*, 2021, **12**, 4917–4927.
20 M. Ohashi, M. Aoki, K. Yamanaka, K. Nakajima, T. Ohsuna, T. Tani and S. Inagaki, *Chem. – Eur. J.*, 2009, **15**, 13041–13046.
21 J. Cravillon, R. Nayuk, S. Springer, A. Feldhoff, K. Huber and M. Wiebcke, *Chem. Mater.*, 2011, **23**, 2130–2141.
22 K. S. Park, Z. Ni, A. P. Cote, J. Y. Choi, R. Huang, F. J. U. Romo, H. K. Chae, M. O'Keeffe and O. M. Yaghi, *Proc. Natl. Acad. Sci. U. S. A.*, 2006, **103**, 10186–10191.
23 V. Glembockyte, M. Frenette, C. Mottillo, A. M. Durantini, J. Gostick, V. Strukil, T. Friscic and G. Cosa, *J. Am. Chem. Soc.*, 2018, **140**, 16882–16887.
24 J. Deng, K. Wang, M. Wang, P. Yu and L. Mao, *J. Am. Chem. Soc.*, 2017, **139**, 5877–5882.
25 Y. Huang, Z. Wang, Z. Chen and Q. Zhang, *Angew. Chem., Int. Ed.*, 2019, **58**, 9696–9711.
26 H. Ye, G. Liu, S. Liu, D. Casanova, X. Ye, X. Tao, Q. Zhang and Q. Xiong, *Angew. Chem., Int. Ed.*, 2018, **57**, 1928–1932.
27 S. M. Pinto, H. D. Burrows, M. M. Pereira, S. M. Fonseca, F. B. Dias, R. Mallavia and M. J. Tapia, *J. Phys. Chem. B*, 2009, **113**, 16093–16100.